

Globally increased cropland soil exposure to climate extremes in recent decades

Received: 10 October 2024

Accepted: 25 April 2025

Published online: 10 May 2025



Luwei Feng ^{1,2,3,4}, Yumiao Wang⁵, Rasmus Fensholt ⁶, Xiaoye Tong ⁶,
Torbern Tagesson ⁷, Xiaoxin Zhang ⁸, Jonas Ardö ⁷, Jie Zhou ⁹,
Wenxuan Shao¹, Yujie Dou¹, Yirong Sang¹ & Feng Tian ^{1,2,3,4} ✉

Soil quality is fundamental to nutrient-rich food production and the sustainability of terrestrial ecosystems. However, inappropriate agricultural practices often lead to persistent soil exposure to air and sunlight, which increases soil organic matter losses and erosion risks, particularly under climate extremes. Here, we provide a satellite-based mapping of daily soil exposure occurrence across global croplands from 2001 to 2022 and evaluate the associated degradation risks caused by extreme climate events. We find that while 57% of global croplands experienced a reduction in soil exposure duration in the past two decades, 86% are increasingly subjected to climate extremes. The areas exposed to increasing climate extremes tend to have higher soil organic carbon levels, indicating an intensified degradation risk of global nutrient-rich cropland soils. Our study offers spatio-temporally explicit insights into global cropland soil exposure and its vulnerability to climate extremes, providing evidence to support improvements in sustainable agriculture practices.

Soil is the foundation for food production and carbon sequestration^{1–3}. Upon decades of accelerated human exploitation, soil quality has been decreasing rapidly worldwide⁴, currently ranging from levels of only fair to poor or even very poor⁵. Nearly half of global croplands suffer from varying degrees of degradation, mainly due to improper agricultural practices, among which conventional tillage often leave soil directly exposed to sunlight and air during cropping phases of initial growth, post-harvest, and fallowing^{6,7}. The absence of protective cover, such as vegetation canopy, crop residue, and snow cover, increases the risk of soil erosion and losses of soil organic carbon and microorganisms, particularly under climate extremes^{8,9}.

To restore degraded soils and ensure agricultural sustainability, a wide range of conservation practices, including reduced tillage, cover

cropping, and mulching, have been implemented through soil conservation projects such as the European Union's Soil Strategy for 2030 and the Environmental Quality Incentives Program. Additionally, perennial crops, by simulating the vegetation of natural ecosystems, are expected to provide year-round protection for the soil and promote the formation of soil organic matter^{8,10}. The effectiveness of these agricultural practices has been evaluated through site-based studies^{11–13}. At a broader scale, cropland soil exposure level has been recognized as an indicator of soil health status^{14–16}. However, the accuracy of existing studies in capturing variations in soil exposure has been constrained, particularly when cropping phases shift rapidly. Furthermore, we still lack a quantitative, spatiotemporally continuous evaluation of soil exposure across global cropland areas.

¹Hubei Key Laboratory of Quantitative Remote Sensing of Land and Atmosphere, School of Remote Sensing and Information Engineering, Wuhan University, Wuhan, China. ²Perception and Effectiveness Assessment for Carbon-neutrality Efforts, Engineering Research Center of Ministry of Education, Institute for Carbon Neutrality, Wuhan University, Wuhan, China. ³Hubei Luojia Laboratory, Wuhan University, Wuhan, China. ⁴State Key Laboratory of Information Engineering in Surveying, Mapping and Remote Sensing, Wuhan University, Wuhan, China. ⁵Department of Geography and Spatial Information Techniques, Ningbo University, Ningbo, China. ⁶Department of Geosciences and Natural Resource Management, University of Copenhagen, Copenhagen, Denmark. ⁷Department of Physical Geography and Ecosystem Science, Lund University, Lund, Sweden. ⁸Future Urbanity & Sustainable Environment (FUSE) Lab, Division of Landscape Architecture, Faculty of Architecture, The University of Hong Kong, Hong Kong Special Administrative Region, Hong Kong, China. ⁹Key Laboratory for Geographical Process Analysis & Simulation of Hubei Province, College of Urban and Environmental Sciences, Central China Normal University, Wuhan, China. ✉e-mail: tian.feng@whu.edu.cn

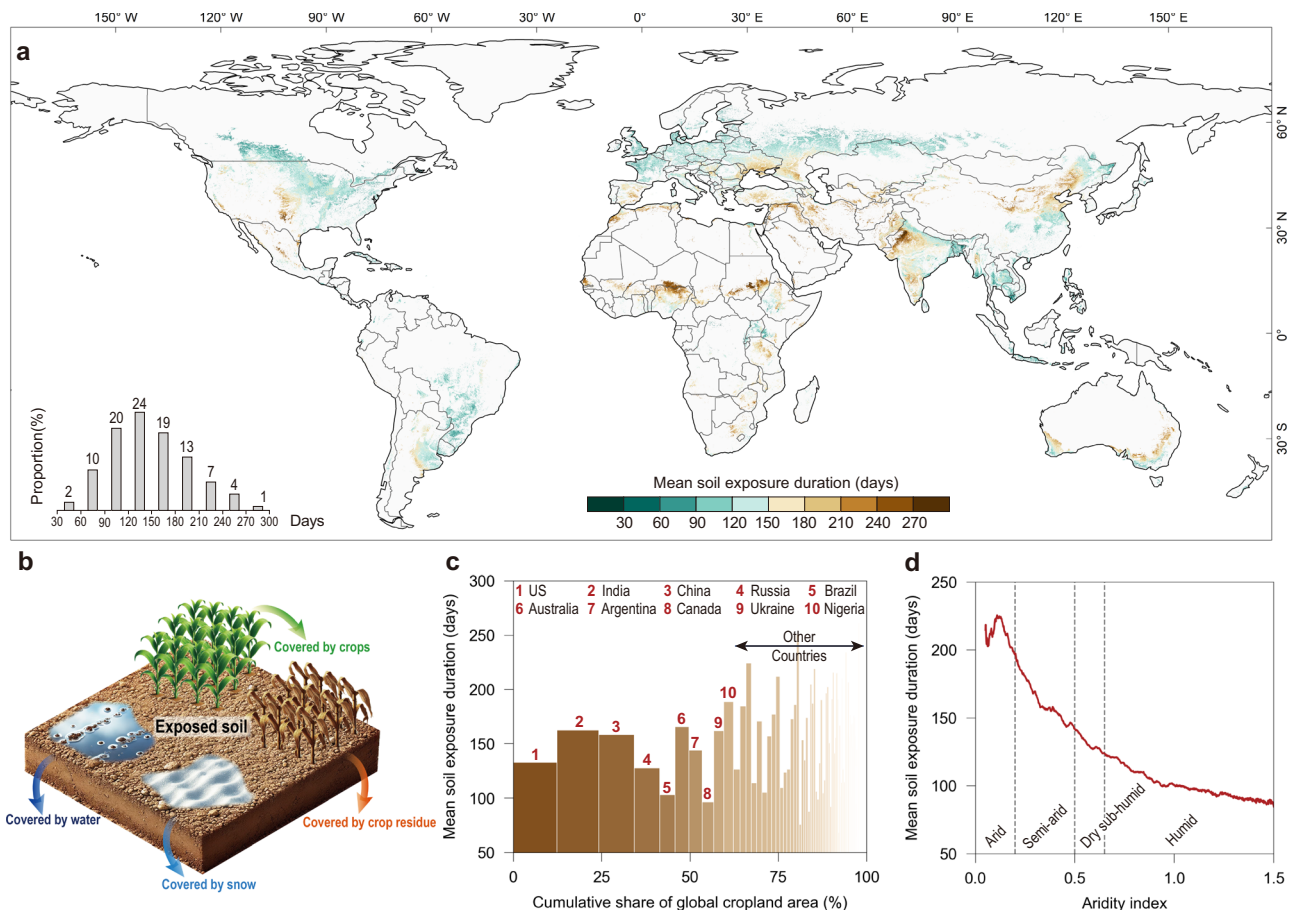


Fig. 1 | Average annual duration of cropland soil exposure during 2001–2022.

a Global map of cropland soil exposure duration at 500 m resolution. Pixels identified as cropland for any given year are retained. The insert shows the distribution of cropland area proportions by exposure duration. **b** Schematic

representation of cropland soil exposure. **c** The cropland soil exposure duration aggregated to the country level. We refer to Supplementary Data 1 for the complete list. **d** The cropland soil exposure duration as a function of global aridity⁶¹.

Changes in frequency and intensity of climate extremes are exerting substantial impacts on soil dynamics¹⁷. Heatwaves, characterized by high air temperatures and land surface solar radiation loads, can either accelerate soil microbial respiration or impair microbial survival, resulting in faster carbon losses^{18,19}. Heavy rainfall and strong winds contribute to soil erosion, depleting topsoil and nutrients²⁰. These effects are especially pronounced under bare soil conditions. The impact of climate extremes on soil conditions is globally heterogeneous^{17,21}. Therefore, a spatiotemporally continuous assessment of soil degradation risks under climate extremes is needed for efficient protection and management of global cropland soils.

Here, we quantify the daily bare soil fraction across global croplands at a spatial resolution of 500 m using satellite observations from Moderate Resolution Imaging Spectroradiometer (MODIS) and Sentinel-2 (Methods, Supplementary Figs. 1–4). We further calculate the annual duration of cropland soil exposure from 2001 to 2022, based on which we evaluate temporal trends of soil degradation risks due to direct exposure to climate extremes.

Results

Global pattern of cropland soil exposure duration

From 2001 to 2022, soils in global croplands were on average exposed (i.e., left without any crops, crop residue, snow, or water cover, Methods) for approximately 147 days per year (Figs. 1a, b, and Supplementary Data 1). About 5% of all cropland experiences soil exposure exceeding eight months, predominantly located in the Sahel region of

Africa and the Great Indian Desert, with the longest durations of soil exposure in Niger and Sudan, lasting 251 and 224 days, respectively (Fig. 1a, and Supplementary Data 1). In contrast, around 12% of global croplands are exposed for less than three months per year, mainly found in America, Europe, Southeast Asia, and Northeastern South Asia (Fig. 1a). The Philippines and Indonesia in Southeast Asia show the shortest cropland soil exposure periods, with average durations of 68 and 76 days, respectively (Supplementary Data 1). Among the top 10 countries by cropland area in 2022, Nigeria has the longest average soil exposure duration at 189 days, while Canada has the shortest at 97 days (Fig. 1c).

The distribution pattern intricately covaries with local climate conditions (Fig. 1d). In particular, croplands in arid and semi-arid climate zones tend to have longer periods of soil exposure, whereas those in humid climates often experience shorter exposure duration. The limited exposure duration in high-latitude regions, such as Canada, the border area between Russia and Kazakhstan, and northeastern China, is largely due to prolonged snow cover, which can last over three months (Supplementary Fig. 5a). We found a discernible negative correlation between cropland soil exposure duration and the length of the growing period reported by Food and Agriculture Organization (Methods and Supplementary Fig. 6). This correlation is less evident in conservation agriculture, where crop residues often remain on the soil surface during the off-growing season, and in high-latitude regions, where prolonged snow cover disrupts the relationship (Methods, Supplementary Fig. 5a).

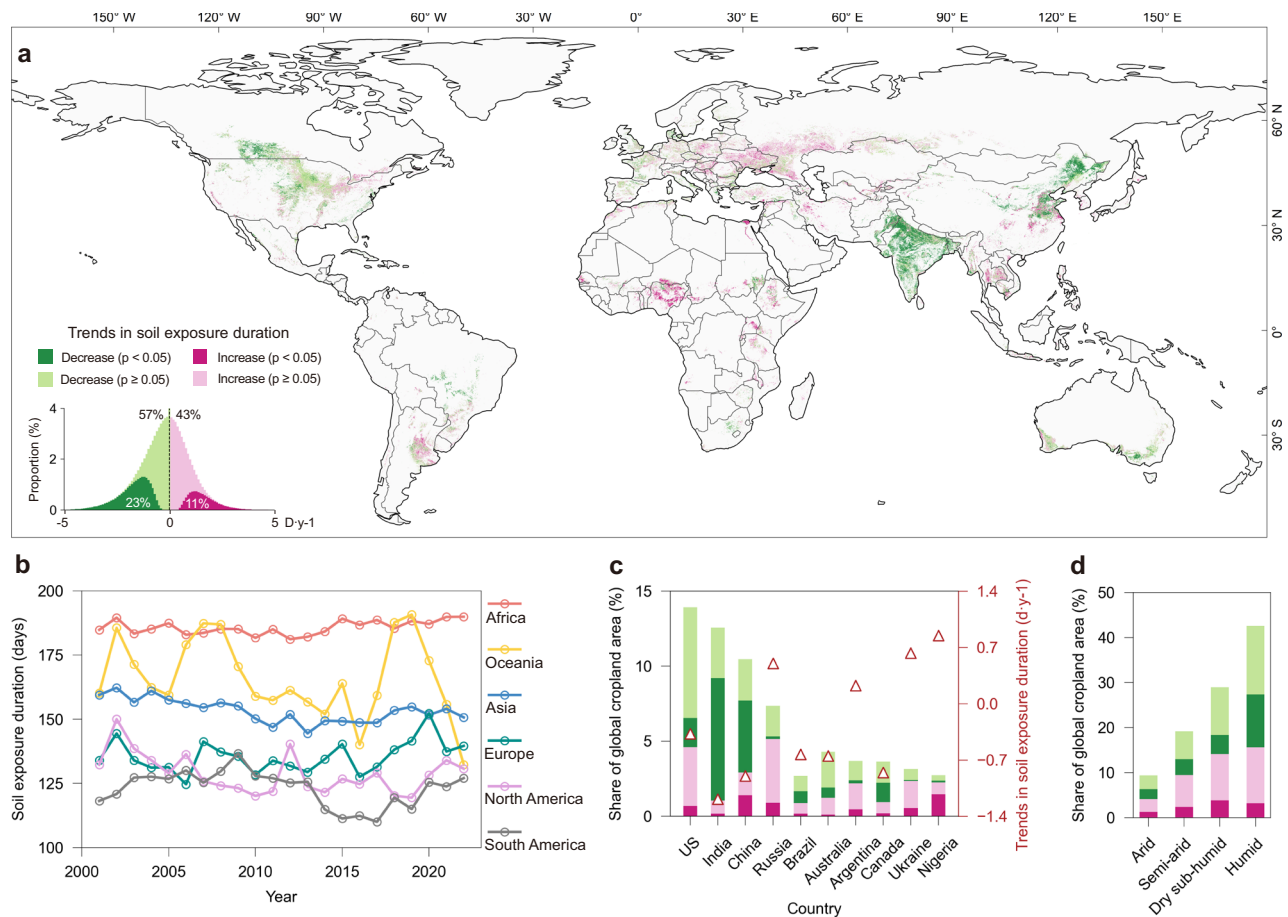


Fig. 2 | Trends in duration of cropland soil exposure during 2001–2022.

a Global map of trends in cropland soil exposure duration at 500 m resolution. Only pixels identified as cropland for all years are retained for the trend analysis. The insert shows the distribution of cropland area proportions with different exposure trends. **b** The cropland soil exposure duration across six continents

during 2001–2022. **c** Share of global cropland for the trends in cropland soil exposure duration among the top 10 countries by cropland area in 2022. **d** Share of global cropland for the trends in cropland soil exposure duration among four aridity conditions⁶¹.

Global trends in cropland soil exposure during 2001–2022

About 57% of croplands experienced a reduction in annual soil exposure duration from 2001 to 2022, with 23% of these reductions being significant ($p < 0.05$) (Fig. 2a). The areas with the largest reductions in exposure duration are mainly located in India, North America, and China, which together account for more than half of the global decrease in cropland exposure (Supplementary Data 1). India is particularly noteworthy, with 92% of its stable cropland areas undergoing reduced soil exposure duration (65% significant at $p < 0.05$), accounting for over 20% of the world's croplands with a shortened soil exposure duration. Relative changes were calculated to assess the rate of change in soil exposure duration in 2022 relative to 2001 (Methods, Eq. 11). Asia has experienced a relatively stable decline in cropland soil exposure duration, declining by approximately 13 days (relative change = -8.31%) from 2001 to 2022 (Fig. 2b). Again, India recorded the most substantial decrease, with a reduction of 25 days (relative change = 14.44%) over the last two decades (Fig. 2c), which may be driven by agriculture intensification during recent decades^{14,22}.

On the other hand, about 43% of croplands saw an increase in annual soil exposure duration, with 11% being statistically significant ($p < 0.05$). Notably, Eastern Europe exhibited a significant increasing trend in cropland exposure, accounting for approximately 20% of the world's cropland with prolonged soil exposure durations. In Africa, cropland soil exposure is also apparent with a cumulative increase of 8 days, representing a relative change of 4.62%. This trend is

particularly pronounced in Uganda, Senegal, Chad, and Nigeria, where more than 80% of cropland areas show increased soil exposure duration. Specifically, Uganda experienced an average increase in soil exposure duration of 28 days (relative change = 26.20%) from 2001 to 2022.

We combined crop cover and crop residue cover, and determined the annual duration of crop/crop residue cover by subtracting the snow cover duration and soil exposure duration from the total number of days in each year. Then, we compared the influence of this combined cover with that of snow cover in determining soil exposure across the Northern Hemisphere (Methods, Figs. 2a, and Supplementary Fig. 5b, c). The increases in both snow and crop/crop residue coverage have contributed to a reduction in cropland soil exposure in northeastern China. In Canada, an increase in snow cover alongside a decrease in crop/crop residue cover is observed. The impact of the snow cover changes is particularly evident, leading to a marked decrease in exposed cropland throughout the region (Supplementary Figs. 5b, d). Conversely, in Nebraska and Kansas in the central U.S., there has been a decrease in snow cover coupled with an increase in crop/crop residue cover. In these regions, the influence of crop/crop residue is more pronounced, resulting in reduced exposure time in most areas. Moreover, in humid regions, the area experiencing a reduction in cropland soil exposure far exceeds that with an increase, whereas in other aridity conditions, no notable differences are observed (Fig. 2d).

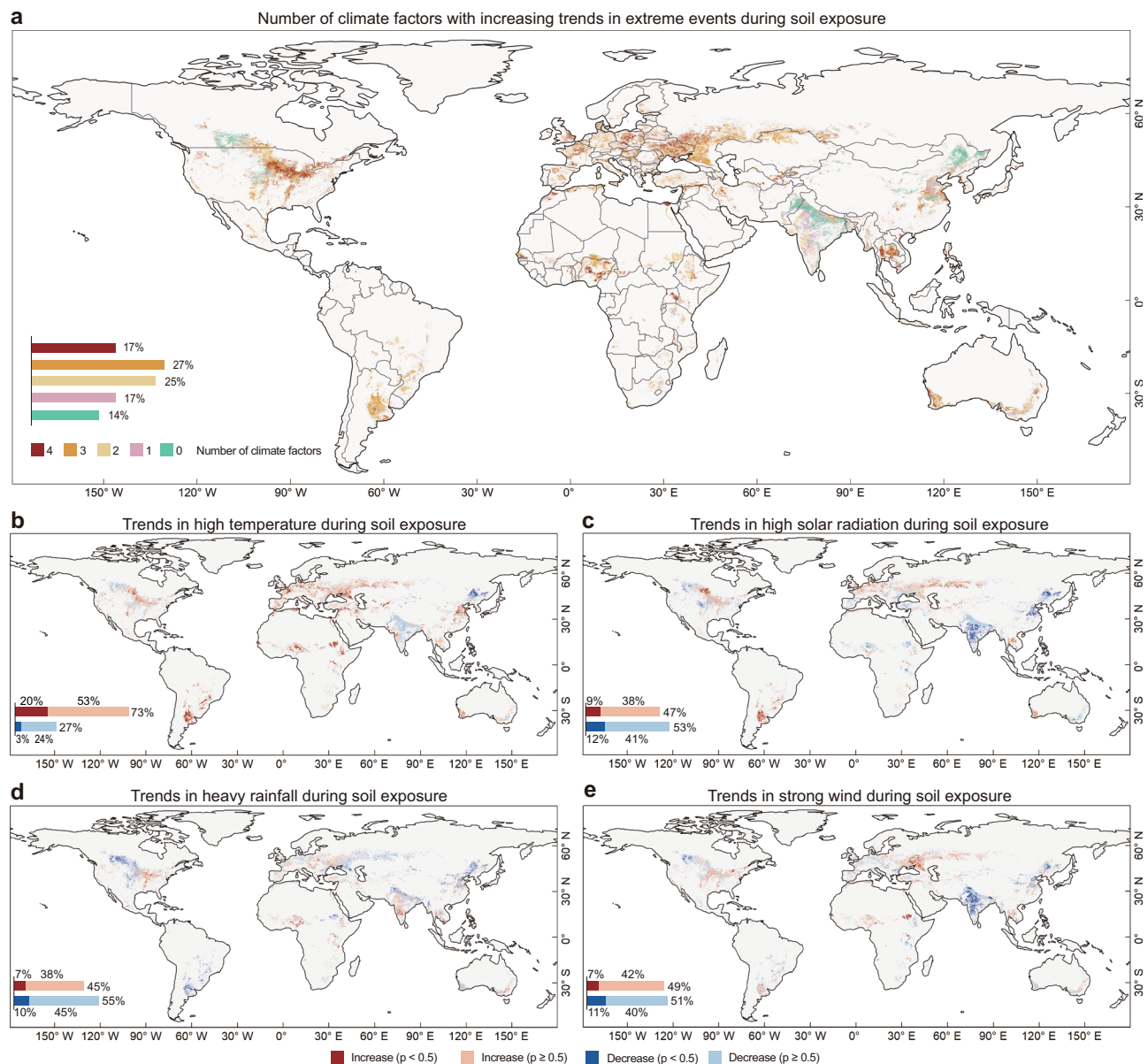


Fig. 3 | Trends in cropland soil exposure to climate extremes during 2001–2022. a Number of climate factors with increasing trends in extreme events during soil exposure. **b–e** Trends in cropland soil exposed to high temperature,

high solar radiation, heavy rainfall, and strong wind, respectively. The inserts show the areal proportion of cropland areas with increased and decreased exposure to climate extremes.

Increasing global cropland soil exposure to climate extremes

We calculated the number of extreme climate events (high temperature, high solar radiation, heavy rainfall, and strong wind) during periods of exposed soil conditions to quantify the risk of soil degradation (Methods). From 2001 to 2022, the extent of cropland soils exposed to climate extremes have changed substantially (Fig. 3). Around 86% of global cropland areas have seen an increase in soil exposure due to the various climate extremes examined during the exposure periods (Fig. 3a). Notably, 17% have experienced an increased risk of exposure to all four types of climate extremes, with the most affected regions located in the U.S. and Europe. Only 14% of global cropland areas have seen a decrease in exposure to all four climate extremes, primarily located in northern India, northeastern China, and Canada.

In particular, 73% of exposed soils of global croplands experienced an increased frequency of high-temperature events from 2001 to 2022 (Fig. 3b). The remaining 27% areas experiencing a decreased frequency of high-temperature events are mainly located in India,

northeastern China, and Canada. On average, there has been an increase of about four days experiencing extreme atmospheric heat to exposed soils across global croplands (Supplementary Table 1). Areas with decreased solar radiation exposure outweigh those with increases by 6%, with notable increases in Europe, South America, and along the border between the U.S. and Canada (Fig. 3c). A similar trend is observed with extreme rainfall, where areas with decreased exposure outweigh those with increases by 10% (Fig. 3d). The exposure to strong wind is relatively balanced between increases and decreases, with significant increases along the Russia-Ukraine border and in Sudan, Africa (Fig. 3e).

Higher soil exposure to climate extremes in SOC-rich croplands

Cropland soil quality varies substantially worldwide, with higher-quality soils offering enhanced productivity, greater soil microbiome diversity, and superior carbon sequestration capabilities⁵. We used soil organic carbon (SOC) as a proxy for soil quality due to its close association with soil fertility, water-holding capacity, and structure^{23–25}. We

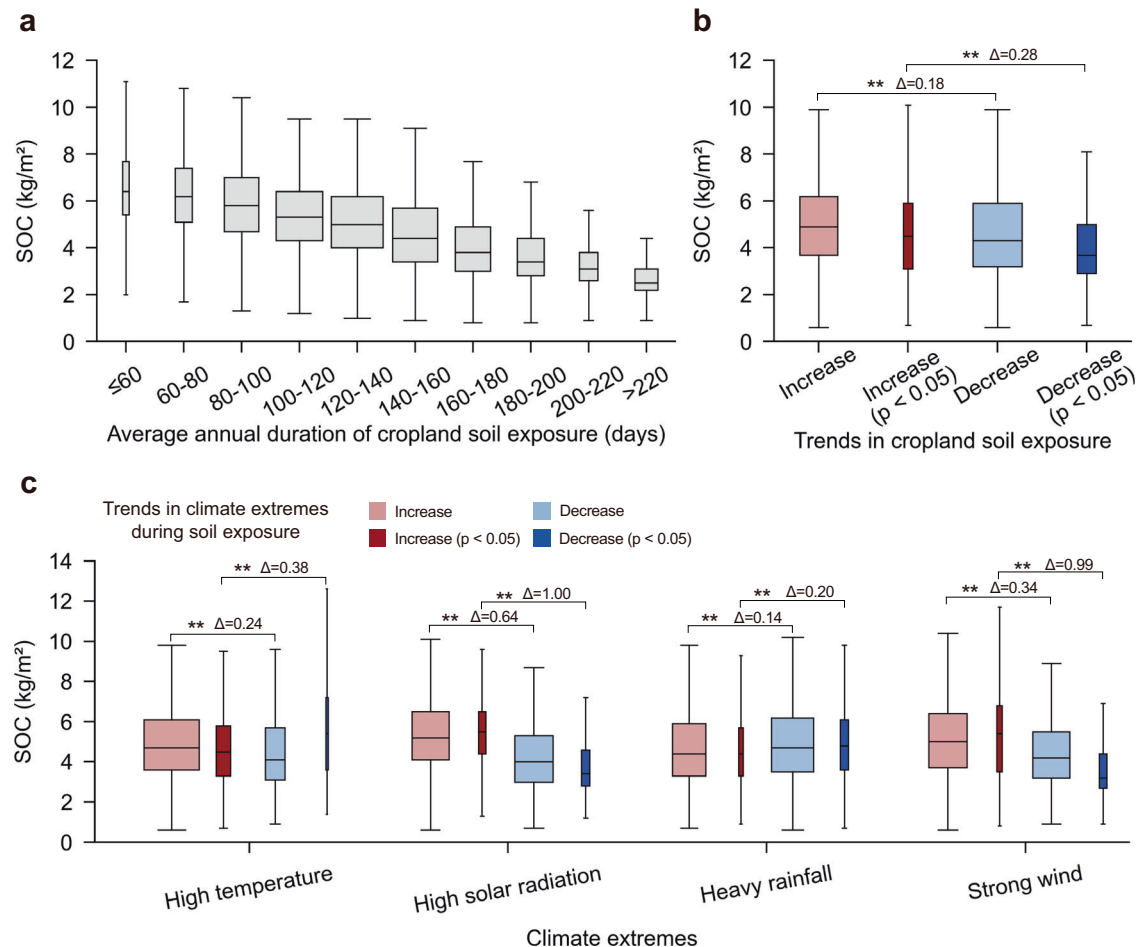


Fig. 4 | Statistics on soil organic carbon (SOC) for areas grouped by different cropland soil exposure conditions. a SOC grouped by the average annual duration of soil exposure. **b** SOC grouped by positive and negative trends in soil exposure during 2001–2022. **c** SOC grouped by positive and negative trends in soil exposure to climate extremes from 2001–2022. In boxplots, the horizontal lines,

from bottom to top, represent the minimum, first quartile, median, third quartile, and maximum values, respectively. The width of the boxes in each box plot represents the number of pixels. ** indicates that the differences in SOC between groups were tested using Welch's t-test, with $p < 0.05$. Δ represents that the magnitude of difference between groups were tested using Glass's Delta.

then analyzed soil exposure-induced degradation risks in global croplands. Global cropland SOC content typically ranges from 2 to 9 kg m⁻², with an average value of 4.8 kg m⁻² (Supplementary Fig. 7)²⁶.

As expected, our results show higher SOC content in croplands with shorter exposure duration (Fig. 4a). Notably, SOC content was significantly higher in croplands where soil exposure increased from 2001 to 2022, compared to those with a decreased soil exposure (Fig. 4b). The average difference in SOC between areas with significant increases and decreases in soil exposure is relative low (0.46 kg m⁻², Glass's Delta = 0.28). However, even small changes in SOC (0.1 kg m⁻² y⁻¹) were found to be correlated with increased food grain production (32 billion kg y⁻¹)²⁷. Moreover, cropland soils exposed to increased climate extreme conditions all have significantly higher SOC levels (Welch's t-test, $p < 0.05$) than those exposed to decreased climate extreme conditions, except for heavy rainfall (Fig. 4c). This indicates that more croplands experienced a decrease than an increase in soil exposure duration, but it did not necessarily correspond to a reduced risk of SOC loss. When considering regions with significant trends in exposure-induced risks, the differences in SOC between areas with increased and decreased soil exposure to high solar radiation and heavy wind are even larger. Therefore, global cropland soils possibly experienced an increased SOC loss due to heightened exposure to climate extremes over the past two decades.

Discussion

Soil is the foundation for life on Earth. In 1994, the United Nations Convention to Combat Desertification (UNCCD) was founded to protect and restore Earth's land, following two high-level UN conferences in 1977 and 1992 on land degradation and desertification. The first task is to assess where and how severely Earth's land has degraded. Satellite remote sensing provides suitable, global, and spatiotemporally consistent data for the assessment. Current remote sensing-based studies use changes in vegetation greenness as a proxy for land degradation assessment, and in the past decades, satellite observations show that the Earth is greening due to climate change and land management^{22,28,29}. However, land degradation is about soil quality rather than vegetation greenness, and ground surveys show that soil quality has declined due to extensive agriculture practices^{7,30}. Instead of assessing vegetation greenness, our study mapped bare soil fraction in global croplands as a proxy for land degradation risk. Also, daily estimation of soil exposure is essential for accurately determining bare land duration and exposure risks to climate extremes, as both land management and weather conditions can change rapidly over time.

We produced a global, daily, and wall-to-wall map of cropland soil exposure over the past two decades and reported an increased cropland soil degradation risk due to direct exposure to more frequent climate extremes during 2001–2022, which has not been documented

before. India, in particular, showed a marked decrease in soil exposure regarding spatial extent and temporal duration, consistent with findings of a strong greening trend^{14,22}. The reduction in soil exposure is largely attributed to agricultural intensification, characterized by heightened cropping frequency and density^{31,32}. This trend is likely to be substantiated by the rise in global population and food demand/production^{33,34}. U.S. has experienced a substantial decrease in cropland soil exposure, potentially attributable to the widespread adoption of cover crops since 2005³⁵. For example, Southern Pennsylvania has experienced an increase of the proportion of winter cover crops from 2010 to 2013, driven by ongoing efforts to promote their adoption³⁶. Concurrently, the duration of cropland soil exposure has decreased (Supplementary Fig. 8), reflecting the positive impact of these initiatives. In addition to the U.S., many high-income countries have already begun to integrate cover crops into their farming practices to address soil erosion, nutrient leakage, control pests and diseases, and boost carbon storage^{37,38}. Beyond cover cropping, perennial grain agriculture also holds potential as an effective means to reduce soil disturbance and degradation⁸. Additionally, changes in snow cover also affect the exposure of soils in croplands at higher latitudes (Figs. 2a, and Supplementary Fig. 5b). While a general decrease in snow cover in the Northern Hemisphere has resulted in an increase in bare land^{39,40}, there are notable exceptions, such as the crop-growing areas in Canada and Northeast China, where an increase in snow cover has correspondingly decreased soil exposure.

Soil exposure in croplands appears to be influenced by a country's level of economic development and degree of political stability. We observed a substantial difference in the duration of soil exposure across an area within approximately 10 km of the Turkey–Syria border (Supplementary Figs. 9a, b). The difference observed is likely associated with the different levels of economic development between the regions. Specifically, the prolonged conflict in Syria has severely damaged agricultural infrastructure, including irrigation systems⁴¹. The variance of annual cropland soil exposure in Syria (std=17.93) is higher than that of Turkey (std=15.42) (Supplementary Fig. 9c). This difference may be attributed to the less developed agricultural practices in Syria to mitigate climate conditions.

In the context of ongoing climate change, more cropland soils have experienced escalated risks of degradation (Fig. 3a). Extreme heat has emerged as the primary threat to bare soils in croplands over the past two decades (Fig. 3b). Only 14% of all global cropland areas remain unaffected by increases in any of four climate extremes examined during soil exposure. These regions are primarily located in northern India, northeastern China, which have witnessed substantial reductions in soil exposure (Fig. 2a). Yet, climate extremes, including heatwaves and extreme precipitation, are projected to increase with ongoing global warming^{42,43}. With extreme rainfall projected to intensify further in India⁴⁴, the risk of soil exposure to heavy rainfall is likely to increase accordingly.

Cropland soil quality exhibits widespread global variations^{5,23}. Consequently, the potential damage caused by soil exposure has varying impacts on the global food supply and environmental health. Specifically, damage to higher-quality soils is likely to cause greater crop yield and soil carbon losses compared to lower-quality soils. Our analysis indicates that regions with increasing trends in cropland soil exposure tend to feature higher SOC levels. Additionally, areas with pronounced risks from climate extremes also show higher SOC values (Fig. 4b, c). Therefore, despite more croplands worldwide have experienced reduced soil exposure compared to increased soil exposure (Fig. 2a), the overall risk of cropland degradation has not necessarily decreased, and crucial functions of croplands such as carbon sequestration and nutrient-rich food production may be adversely affected.

Although maintaining cover over cropland soils can mitigate the detrimental effects of direct exposure to air and sunlight, the methods

of coverage are crucial, as they potentially introduce additional risks. For example, the observed reduction in cropland soil exposure in the U.S. is likely attributable to the implementation of cover crop strategies, which are expected to retain soil structure, reduce soil erosion, and enhance soil health. Conversely, in India, the current reduction has primarily been achieved through intensive farming, which, paradoxically, may exacerbate soil health deterioration⁴. However, the current method only captures the changes in cropland soil exposure, without identifying the underlying causes. Future research should investigate the specific drivers of cropland soil exposure reduction, allowing for a comprehensive assessment of the risks faced by cropland soils.

Methods

Overview

We introduced a methodology for daily soil exposure mapping across global croplands using satellite imagery (Supplementary Fig. 1). Initially, we selected 34 regions globally, each measuring $0.2^\circ \times 0.2^\circ$, characterized by extensive cropland coverage. We then applied Linear Spectral Mixture Analysis (LSMA)⁴⁵ to generate multi-temporal bare soil fraction data utilizing Sentinel-2-based Normalized Difference Vegetation Index (NDVI) and Normalized Difference Tillage Index (NDTI) time series. The bare soil fraction data, serving as ground truth, was then resampled to align with the spatial resolution of MODIS imagery. Subsequently, a linear regression model correlating resampled bare soil fraction data with MODIS-derived NDVI and NDTI was developed. Employing this model, we mapped daily bare soil fraction from 2001 to 2022. We excluded dates with snow or water cover by thresholding Normalized Difference Snow Index (NDSI) and Automated Water Extraction Index (AWEI)⁴⁶, thereby obtaining precise soil exposure conditions in croplands. We further calculated the annual duration of soil exposure for the same period to assess the temporal trends of potential risks associated with exposure to climate extremes. Additionally, we used SOC as a proxy for soil quality and explored the variations in exposure risks across croplands with differing soil qualities.

The extent of cropland area

The cropland extent was generated from a 30 m time-series global cropland mapping product, comprising five layers at four-year intervals from 2000 to 2019⁴⁷. We then aggregated the 30 m resolution product to 0.0045° by classifying pixels as cropland if more than 50% of the original pixels represent cropland. Our study spans from 2001 to 2022, and for each specific year, we utilized the layer with the nearest year as a mask to derive the cropland extent. For trend analysis, only pixels identified as cropland during all years were retained. For other analyses, pixels identified as cropland for any given year were retained.

Preparation of satellite imagery

We used Sentinel-2 and MODIS satellite imagery to map soil exposure across global croplands. Specifically, MOD09GA data⁴⁸ spanning from 2001 to 2022 were included in the study, and the state_1km quality band was employed to minimize the influence from cloud contamination. The data were originally in a sinusoidal projection at a 500 m spatial resolution, and were converted into a WGS84 geographical projection at a 0.0045° spatial resolution ($\sim 500 \text{ m} \times 500 \text{ m}$ at Equator). Additionally, Sentinel-2 Level-2A data⁴⁹, which is provided in the Universal Transverse Mercator projection, was used in this study for the period from 2019 to 2021. To ensure high quality data, the Scene Classification Layer was utilized to eliminate cloud, snow, and water, with further cloud removal achieved by setting the probability threshold at 50% using the Sentinel-2 Cloud Probability product.

Using the imagery, we calculated four indices, namely NDVI, NDTI, NDSI, and AWEI, known for effectively characterizing the conditions of

crops, crop residue, snow, and water, respectively, using Eqs. (1)–(4).

$$\text{NDVI} = \frac{\text{NIR} - \text{RED}}{\text{NIR} + \text{RED}} \quad (1)$$

$$\text{NDTI} = \frac{\text{SWIR1} - \text{SWIR2}}{\text{SWIR1} + \text{SWIR2}} \quad (2)$$

$$\text{NDSI} = \frac{\text{GREEN} - \text{SWIR1}}{\text{GREEN} + \text{SWIR1}} \quad (3)$$

$$\text{AWEI} = 4 \times (\text{GREEN} - \text{SWIR1}) - (0.25 \times \text{NIR} + 2.75 \times \text{SWIR2}) \quad (4)$$

Selection of representative regions for model building

To enhance the robustness of the bare soil fraction estimation model across space and crop types, we selected 34 regions globally (Supplementary Data 2), each spanning $0.2^\circ \times 0.2^\circ$. These regions were chosen for their high cropland density and considerable variation in dominant crop types, with the assistance of multiple crop type data. These data include the Cropland Data Layer (CDL) for 2020 released by the United States Department of Agriculture (USDA)⁵⁰, the Agriculture and Agri-Food Canada (AAFC) crop type digital maps for 2020⁵¹, the ESA WorldCereal product for 2021⁵², the ESA WorldCover data for 2020⁵³, and crop type maps in Northeast China for 2019⁵⁴.

Estimation of bare soil fraction with MODIS-based NDVI and NDTI

Using data from the 34 representative regions, we developed a bare soil fraction estimation model using MODIS-based NDVI and NDTI. Two main steps were involved: calculation of alternatives to ground truth bare soil fraction using Sentinel-2 data, and construction of MODIS-based bare soil fraction estimation model.

Due to the difficulty of obtaining ground measurements for bare soil fraction values, we generated 10-meter resolution bare soil fraction data from Sentinel-2 imagery using LSMA as alternatives to ground truth. LSMA assumes that the observed spectrum of a pixel is a linear combination of the spectra of different pure components, referred to as endmembers, present within that pixel. In cropland ecosystems, endmembers mainly refer to crops, crop residue, and bare soils. In each region, we randomly selected 1500 Sentinel-2 pixels and excluded non-dominant crop areas based on the aforementioned crop type data (Supplementary Data 2). Then, we extracted the NDVI and NDTI values for the remaining points using the 5-day median composites of Sentinel-2 imagery corresponding to the years of the crop type data. The valid data from all the remaining points across all timestamps were aggregated to derive the NDVI-NDTI matches for each region. Based on the triangular space method (Supplementary Fig. 2), we constructed a two-dimensional scatter plot, commonly referred to as the triangular space, using NDVI-NDTI matches for each region. Within each plot, we visually determined the vertices of the triangular space (Supplementary Fig. 3), which symbolize pure pixels of crops, crop residue, and bare soils. The values of NDVI and NDTI corresponding to the vertices were taken as the spectral features of endmembers in each region (Supplementary Data 2). Finally, the Sentinel-2-based bare soil fraction could be determined by LSMA using Eq. (5):

$$\begin{aligned} \text{NDVI}_m &= \text{CF} \times \text{NDVI}_c + \text{CRF} \times \text{NDVI}_{cr} + \text{BSF} \times \text{NDVI}_{bs} \\ \text{NDTI}_m &= \text{CF} \times \text{NDTI}_c + \text{CRF} \times \text{NDTI}_{cr} + \text{BSF} \times \text{NDTI}_{bs} \\ \text{CF} + \text{CRF} + \text{BSF} &= 100\%, 0 \leq \text{CF} \leq 100\%, 0 \leq \text{CRF} \leq 100\%, 0 \leq \text{BSF} \leq 100\% \end{aligned} \quad (5)$$

where NDVI_m and NDTI_m represent the NDVI and NDTI values of a mixed pixel. NDVI_c , NDVI_{cr} , and NDVI_{bs} are the NDVI values of crop,

crop residue, and bare soil endmembers, respectively. NDTI_c , NDTI_{cr} , and NDTI_{bs} are the NDTI values of crop, crop residue, and bare soil endmembers, respectively. CF, CRF, and BSF denote the proportions of crops, crop residue, and bare soils in a mixed pixel.

In the second step, we aim to formulate the bare soil fraction estimation model using MODIS-based NDVI and NDTI. To achieve this, we first computed the cloud proportion in 5-day median composites of MODIS and Sentinel-2 imagery for each selected region spanning from 2019 to 2021, identifying timestamps when the cloud cover was below 50%. Then, we generated the MODIS-based NDVI and NDTI for the chosen timestamps of these regions. And the Sentinel-2-based bare soil fraction data was resampled to 0.0045° by averaging aggregation. Within each region, 1000 points were randomly generated, and MODIS-based NDVI and NDTI values were extracted at each timestamp as independent variables, with corresponding resampled bare soil fraction values extracted as dependent variables. Multiple linear regression was used to model the relationship between bare soil fraction and MODIS-based NDVI and NDTI. To enhance the reliability of our results, we employed the leave-one-out cross-validation strategy. In this approach, the data from each of the 34 selected regions is individually used as the test set in a single iteration, with the data from the other regions serving as the training set. The resulting regression coefficients and accuracy for each iteration are detailed in Supplementary Data 3 and Supplementary Fig. 10. By averaging the 34 sets of regression coefficients, we derived the regression equation for modeling the global bare soil fraction (Eq. 6). Using the equation, the final accuracy was calculated by incorporating all data from the 34 selected regions, resulting in coefficient of determination (R^2), root mean squared error (RMSE), and mean absolute error (MAE) of 0.73, 13.61%, and 10.69%, respectively.

$$\text{BSF} = 36 \times \text{NDVI} - 268 \times \text{NDTI} + 90 \quad (6)$$

Spatiotemporal mapping of cropland bare soil

To acquire the spatiotemporal distribution of bare soils in croplands, non-cropland pixels were excluded using the previously mentioned resampled cropland extent. Then, we extracted the daily values of NDVI, NDTI, NDSI, and AWEI⁴⁶ during 2001–2022 from MODIS imagery. Due to the impact of cloud cover and atmospheric perturbations, satellite observations frequently exhibit discontinuities. We therefore employed Harmonic Analysis of Time Series (HANTS)^{55–57}, a time series reconstruction algorithm, to fit the four indices of each pixel based on the annually available observations, ensuring the generation of temporally continuous data. Employing principles reminiscent of Fourier analysis, HANTS is able to decompose complex time series datasets into distinct harmonic components, each representing a unique frequency or periodicity. HANTS can be expressed by the Eq. (7).

$$y_{t_j} = a_0 + \sum_{i=1}^N \left[a_i \sin(2\pi f_i t_j) + b_i \cos(2\pi f_i t_j) \right] \quad (7)$$

where y_{t_j} represents the reconstructed value of pixel j at time t . a_0 is the coefficient at zero frequency. a_i and b_i are coefficients of the trigonometric components associated with the frequencies f_i . N is the number of harmonic components and is set to 4 in this study. After employing HANTS to generate annually reconstructed time series of NDVI, NDTI, NDSI, and AWEI, the daily bare soil fraction for each pixel from 2001 to 2022 was computed based on Eq. (6). It is worth noting that, due to winter snow cover in high latitudes, we used NDSI to identify snow for areas north of 35°N from November to March. Pixels with NDSI values above 0.4 were considered as snow, leading to a corresponding bare soil fraction value of 0. For areas north of 35°N from April to October and in other regions where the soil in rice cultivation regions is periodically covered by water, we used AWEI for

water identification. Pixels with AWEI values exceeding 0 were designated as water-covered, resulting in the corresponding bare soil fraction being set to 0. Utilizing the method described above, we calculated the daily bare soil fraction for global cropland pixels spanning from 2001 to 2022 (Supplementary Fig. 4). We determined the annual duration of cropland soil exposure by aggregating the bare soil fraction values for all days of the year. We further calculated the average annual duration of cropland soil exposure and analyzed trends in exposure duration using the slopes of linear regression equations.

Quantifying the risk of exposure to climate extremes

An extreme climate event is defined as a day with a meteorological variable value surpassing the 90th percentile⁵⁸ between 2001 and 2022. In this study, we considered four meteorological variables, namely mean daily surface temperature, mean daily surface solar radiation downwards, daily total rainfall, and mean daily wind speed. These meteorological variables were extracted from ERA5-Land, a global land reanalysis dataset provided by the European Centre for Medium-Range Weather Forecasts⁵⁹. The dataset provides hourly land surface variables on a regular grid with a spatial resolution of $0.1^\circ \times 0.1^\circ$, and it was further resampled to a spatial resolution of 0.0045° using the nearest neighbor method.

We quantified the risk of exposure to climate extremes by evaluating the length of time each year that cropland soil was exposed to climate extremes, as shown in Eq. (8).

$$R^{i,y,t} = \sum_{d=1}^{D^y} F_d^{i,y,t} E_d^{i,y,t} \quad (8)$$

where $R^{i,y,t}$ represents the risk of exposure characterized by extreme weather t of pixel i in year y . D^y is the number of days in year y , and d is the day of year (DOY). F_d denotes the bare soil fraction on DOY d . E_d denotes whether extreme climate events occurred on DOY d , with values of either 0 or 1. The trends in risk of exposure were considered to be linear and were represented by the slopes.

Quantifying the relationship between SOC and exposure

We used the SOC content obtained from SoilGrids version 2.0²⁶ to represent the quality of cropland soils. The original data, with a spatial resolution of 250 m, was converted to a geographic resolution of 0.0045° by averaging aggregation to match the spatial resolution of MODIS-based bare soil fraction data. We investigated the relationship between SOC content and the average annual duration of cropland soil exposure. Additionally, we compared SOC content across regions with increased versus decreased soil exposure durations and between regions with heightened versus reduced exposure-induced risks.

Statistics by country

We conducted a statistical analysis of six continents and the top 50 countries of the largest cropland areas in 2022 (Supplementary Data 1). This analysis encompasses a range of critical indicators, including the average annual exposure duration (Eq. 9), the average change in exposure duration (Eq. 10), the average relative change in exposure duration (Eq. 11), the area with decreased exposure (Eq. 12), the area with increased exposure duration (Eq. 13), the proportion of areas with decreased exposure (Eq. 14), the proportion of areas with increased exposure (Eq. 15).

$$\text{Average annual exposure duration} = \frac{\sum_{i=1}^n A_i \bar{D}_i}{\sum_{i=1}^n A_i} \quad (9)$$

$$\text{Average change in exposure duration} = \sum_{i=1}^{n_s} T_i A_i / N \quad (10)$$

Average relative change in exposure duration =

$$\frac{\sum_{i=1}^n A_i \hat{D}_{2022} - \sum_{i=1}^n A_i \hat{D}_{2001}}{\sum_{i=1}^n A_i \hat{D}_{2001}} \quad (11)$$

$$\text{Area with decreased exposure} = \sum_{i=1}^{n^-} A_i \quad (12)$$

$$\text{Area with increased exposure} = \sum_{i=1}^{n^+} A_i \quad (13)$$

$$\text{Proportion of areas with decreased exposure} = \frac{\sum_{i=1}^{n^-} A_i}{\sum_{i=1}^n A_i} \quad (14)$$

$$\text{Proportion of areas with increased exposure} = \frac{\sum_{i=1}^{n^+} A_i}{\sum_{i=1}^n A_i} \quad (15)$$

where A_i is the area of pixel i , \bar{D}_i is the average annual exposure duration of pixel i . \hat{D}_{2001} and \hat{D}_{2022} represent the predicted exposure durations for 2001 and 2022 using the linear regression. T is the trend, expressed as the slope of the linear regression. N represents the years from 2001 to 2022, which is set to 21. n , n_s , n^- , and n^+ represent the number of cropland pixels, the number of stable cropland pixels, the number of pixels with decreased exposure, and the number of pixels with increased exposure, respectively.

Analysis of the impact of snow cover on cropland soil exposure

We explored the impact of snow cover on cropland exposure duration at higher latitudes (north of 35°N) in the Northern Hemisphere using the aforementioned MODIS-based NDSI time series data processed with the HANTS algorithm. Pixels with NDSI values above 0.4 were considered to be snow-covered. We calculated the annual duration of snow cover from 2001 to 2022. The annual duration of crop/crop residue cover was then determined by subtracting the snow cover duration and soil exposure duration from the total number of days in each year. We calculated the correlation between the durations of these two types of cover and the soil exposure duration, identifying the dominant factor as the one with the larger absolute correlation value (Supplementary Fig. 5d).

Correlating bare soil fraction data with growing period data

We used the length of the growing period data, published by Food and Agriculture Organization⁶⁰, to correlate with our assessment of the duration of soil exposure. Length of the growing period is characterized as the number of days when the average daily temperature remains above 5°C and the soil moisture is sufficient to support crop germination and growth. Data from 2001 to 2010 was used because the values prior to 2010 were derived from historical meteorological data, whereas values after 2010 were based on predicted meteorological data. The estimated average annual duration of cropland soil exposure during 2001–2010 was resampled to match the spatial resolution of the length of the growing period data at 5 arc-minute using averaging aggregation. A correlation analysis of the two datasets was performed along the gradient of latitude (Supplementary Fig. 6).

Data availability

The data on annual cropland soil duration and trends are available in Google's Earth Engine App at <https://lwfeng.users.earthengine.app/view/cropland-soil-exposure-explorer>. The daily bare soil fraction in croplands for 2022 is available at <https://doi.org/10.5281/zenodo.14553703>.

Code availability

The code for time series data generation and bare soil fraction calculation is available at <https://doi.org/10.5281/zenodo.14553644>.

References

- Amundson, R. et al. Soil and human security in the 21st century. *Science* **348**, 1261071 (2015).
- Montanarella, L. et al. World's soils are under threat. *Soil* **2**, 79–82 (2016).
- Rumpel, C. et al. The role of soil carbon sequestration in enhancing human resilience in tackling global crises including pandemics. *Soil Security* **8**, 100069 (2022).
- Borrelli, P. et al. An assessment of the global impact of 21st century land use change on soil erosion. *Nat. Commun.* **8**, 2013 (2017).
- Montanarella, L. et al. *Status of the World's Soil Resources (SWSR) – Main Report*. Food and Agriculture Organization of the United Nations and Intergovernmental Technical Panel on Soils, Rome, Italy (FAO and ITPS, 2015). <https://openknowledge.fao.org/server/api/core/bitstreams/6ec24d75-19bd-4f1f-b1c5-5becf50d0871/content>.
- FAO. *The State of the World's Land and Water Resources for Food and Agriculture – Systems at breaking point*. (FAO, 2021).
- Montgomery, D. R. Soil erosion and agricultural sustainability. *Proc. Natl Acad. Sci.* **104**, 13268–13272 (2007).
- Crews, T. E., Carton, W. & Olsson, L. Is the future of agriculture perennial? imperatives and opportunities to reinvent agriculture by shifting from annual monocultures to perennial polycultures. *Glob. Sustainability* **1**, e11 (2018).
- Smith, P. Soils and climate change. *Curr. Opin. Environ. sustainability* **4**, 539–544 (2012).
- Crews, T. E. & Rumsey, B. E. What agriculture can learn from native ecosystems in building soil organic matter: a review. *Sustainability* **9**, 578 (2017).
- He, Y. T. et al. Long-term combined chemical and manure fertilizations increase soil organic carbon and total nitrogen in aggregate fractions at three typical cropland soils in China. *Sci. Total Environ.* **532**, 635–644 (2015).
- Sleutel, S. et al. Carbon stock changes and carbon sequestration potential of Flemish cropland soils. *Glob. Change Biol.* **9**, 1193–1203 (2003).
- Garnier, J. et al. Storage or loss of soil active carbon in cropland soils: the effect of agricultural practices and hydrology. *Geoderma* **407**, 115538 (2022).
- Demattê, J. A. M. et al. Bare Earth's surface spectra as a proxy for soil resource monitoring. *Sci. Rep.* **10**, 4461 (2020).
- Mzid, N., Pignatti, S., Huang, W. & Casa, R. An analysis of bare soil occurrence in arable croplands for remote sensing topsoil applications. *Remote Sens.* **13**, 474 (2021).
- Diek, S., Fornallaz, F., Schaepman, M. E. & De Jong, R. Barest pixel composite for agricultural areas using Landsat time series. *Remote Sens.* **9**, 1245 (2017).
- Wang, M. et al. Responses of soil organic carbon to climate extremes under warming across global biomes. *Nature Climate Change* **14**, 98–105 (2023).
- Hartley, I. P., Hill, T. C., Chadburn, S. E. & Hugelius, G. Temperature effects on carbon storage are controlled by soil stabilisation capacities. *Nat. Commun.* **12**, 6713 (2021).
- Joergensen, R. G., Brookes, P. C. & Jenkinson, D. S. Survival of the soil microbial biomass at elevated temperatures. *Soil Biol. Biochem.* **22**, 1129–1136 (1990).
- Jansson, J. K. & Hofmockel, K. S. Soil microbiomes and climate change. *Nat. Rev. Microbiol.* **18**, 35–46 (2020).
- Wang, M. et al. Global soil profiles indicate depth-dependent soil carbon losses under a warmer climate. *Nat. Commun.* **13**, 5514 (2022).
- Chen, C. et al. China and India lead in greening of the world through land-use management. *Nat. sustainability* **2**, 122–129 (2019).
- Haefele, S. M., Nelson, A. & Hijmans, R. J. Soil quality and constraints in global rice production. *Geoderma* **235**, 250–259 (2014).
- Shukla, M. K., Lal, R. & Ebinger, M. Determining soil quality indicators by factor analysis. *Soil Tillage Res.* **87**, 194–204 (2006).
- Olsson, L. et al. The State of the World's Arable Land. *Annu. Rev. Environ. Resour.* **48**, 451–475 (2023).
- Poggio, L. et al. SoilGrids 2.0: producing soil information for the globe with quantified spatial uncertainty. *Soil* **7**, 217–240 (2021).
- Lal, R. Enhancing crop yields in the developing countries through restoration of the soil organic carbon pool in agricultural lands. *Land Degrad. Dev.* **17**, 197–209 (2006).
- Fensholt, R. et al. Greenness in semi-arid areas across the globe 1981–2007—an Earth observing satellite based analysis of trends and drivers. *Remote Sens. Environ.* **121**, 144–158 (2012).
- Zhu, Z. et al. Greening of the Earth and its drivers. *Nat. Clim. change* **6**, 791–795 (2016).
- Tsiafouli, M. A. et al. Intensive agriculture reduces soil biodiversity across Europe. *Glob. change Biol.* **21**, 973–985 (2015).
- Ray, D. K. & Foley, J. A. Increasing global crop harvest frequency: recent trends and future directions. *Environ. Res. Lett.* **8**, 044041 (2013).
- Hu, Q. et al. Global cropland intensification surpassed expansion between 2000 and 2010: a spatio-temporal analysis based on GlobeLand30. *Sci. Total Environ.* **746**, 141035 (2020).
- Kopittke, P. M., Menzies, N. W., Wang, P., McKenna, B. A. & Lombi, E. Soil and the intensification of agriculture for global food security. *Environ. Int.* **132**, 105078 (2019).
- Ramankutty, N. et al. Trends in global agricultural land use: implications for environmental health and food security. *Annu. Rev. plant Biol.* **69**, 789–815 (2018).
- Wallander, S., Smith, D., Bowman, M., Claassen, R. Cover crop trends, programs, and practices in the United States. (2021).
- Hively, W. D., Duiker, S., McCarty, G. & Prabhakara, K. Remote sensing to monitor cover crop adoption in southeastern Pennsylvania. *J. Soil Water Conserv.* **70**, 340–352 (2015).
- Rivière, C., Béthinger, A. & Bergez, J.-E. The effects of cover crops on multiple environmental sustainability indicators—a review. *Agronomy* **12**, 2011 (2022).
- Jian, J., Du, X., Reiter, M. S. & Stewart, R. D. A meta-analysis of global cropland soil carbon changes due to cover cropping. *Soil Biol. Biochem.* **143**, 107735 (2020).
- Chen, X., Liang, S., Cao, Y., He, T. & Wang, D. Observed contrast changes in snow cover phenology in northern middle and high latitudes from 2001–2014. *Sci. Rep.* **5**, 16820 (2015).
- Zhang, Y. & Ma, N. Spatiotemporal variability of snow cover and snow water equivalent in the last three decades over Eurasia. *J. Hydrol.* **559**, 238–251 (2018).
- Li, X.-Y. et al. Civil war hinders crop production and threatens food security in Syria. *Nat. Food* **3**, 38–46 (2022).
- Morit, A. Extreme heatwaves: surprising lessons from the record warmth. *Nature* **608**, 464–465 (2022).
- de Vries, I., Sippel, S., Zeder, J., Fischer, E. & Knutti, R. Increasing extreme precipitation variability plays a key role in future record-shattering event probability. *Commun. Earth Environ.* **5**, 482 (2024).
- Iles, C. E. et al. Strong regional trends in extreme weather over the next two decades under high-and low-emissions pathways. *Nat. Geosci.* **17**, 845–850 (2024).
- Keshava, N. & Mustard, J. F. Spectral unmixing. *IEEE signal Process. Mag.* **19**, 44–57 (2002).
- Feyisa, G. L., Meilby, H., Fensholt, R. & Proud, S. R. Automated water extraction index: a new technique for surface water mapping using Landsat imagery. *Remote Sens. Environ.* **140**, 23–35 (2014).

47. Potapov, P. et al. Global maps of cropland extent and change show accelerated cropland expansion in the twenty-first century. *Nat. Food* **3**, 19–28 (2022).
48. Vermote E., Wolfe R. MODIS/Terra surface reflectance daily L2G Global 1km and 500m SIN Grid V061. *NASA EOSDIS Land Processes Distributed Active Archive Center* (2021).
49. Main-Knorn, M. et al. Sen2Cor for sentinel-2. Image and Signal Processing for Remote Sensing XXIII; 2017; Warsaw, Poland: SPIE; p. 37–48 (2017).
50. USDA NASS. Cropland Data Layer. (2020).
51. AAFC. Agriculture and Agri-Food Canada Annual Crop Inventory. (2020).
52. Van Tricht, K. et al. WorldCereal: a dynamic open-source system for global-scale, seasonal, and reproducible crop and irrigation mapping. *Earth Syst. Sci. Data Discuss.* **2023**, 1–36 (2023).
53. Zanaga, D. et al. ESA WorldCover 10 m 2020 v100. Zenodo (2021).
54. You, N. et al. The 10-m crop type maps in Northeast China during 2017–2019. *Sci. data* **8**, 41 (2021).
55. Roerink, G. J., Menenti, M. & Verhoef, W. Reconstructing cloudfree NDVI composites using Fourier analysis of time series. *Int. J. Remote Sens.* **21**, 1911–1917 (2000).
56. Zhou, J., Jia, L. & Menenti, M. Reconstruction of global MODIS NDVI time series: performance of harmonic ANALYSIS of time series (HANTS). *Remote Sens. Environ.* **163**, 217–228 (2015).
57. Zhou, J. et al. A scalable software package for time series reconstruction of remote sensing datasets on the Google Earth Engine platform. *Int. J. Digital Earth* **16**, 988–1007 (2023).
58. Masson-Delmotte, V. et al. Climate change 2021: the physical science basis. *Contribution working group I sixth Assess. Rep. inter-governmental panel Clim. change* **2**, 2391 (2021).
59. Muñoz Sabater J. ERA5-Land monthly averaged data from 1981 to present. *Copernicus Climate Change Service (C3S) Climate Data Store (CDS)* (2019).
60. FAO. GAEZ Data Portal. 2021. Data accessed: 23 Dec 2023 <https://gaez.fao.org/pages/data-viewer>.
61. Zomer, R. J., Xu, J. & Trabucco, A. Version 3 of the global aridity index and potential evapotranspiration database. *Sci. Data* **9**, 409 (2022).

Acknowledgements

This research was funded by the National Key Research and Development Program of China (2023YFF1303702, F.T.), the China Postdoctoral Science Foundation (2023M742679, L.F.), the Open Research Fund Program of Key Laboratory of Digital Mapping and Land Information Application, Ministry of Natural Resources (ZRZYBWD202306, L.F.).

Author contributions

F.T. and L.F. designed the study. Y.W., L.F. and W.S. prepared the satellite imagery. J. Z., Y.W. and L.F. developed the code for time series data generation. L.F. performed the data analyses. L.F. drafted the manuscript with editing by F.T., R.F., X.T., T.T., X.Z., J.A., J.Z., Y.D. and Y.S.

Competing interests

The authors declare no competing interests.

Additional information

Supplementary information The online version contains supplementary material available at <https://doi.org/10.1038/s41467-025-59544-1>.

Correspondence and requests for materials should be addressed to Feng Tian.

Peer review information *Nature Communications* thanks José Safanelli and the other, anonymous, reviewer(s) for their contribution to the peer review of this work. A peer review file is available.

Reprints and permissions information is available at <http://www.nature.com/reprints>

Publisher's note Springer Nature remains neutral with regard to jurisdictional claims in published maps and institutional affiliations.

Open Access This article is licensed under a Creative Commons Attribution-NonCommercial-NoDerivatives 4.0 International License, which permits any non-commercial use, sharing, distribution and reproduction in any medium or format, as long as you give appropriate credit to the original author(s) and the source, provide a link to the Creative Commons licence, and indicate if you modified the licensed material. You do not have permission under this licence to share adapted material derived from this article or parts of it. The images or other third party material in this article are included in the article's Creative Commons licence, unless indicated otherwise in a credit line to the material. If material is not included in the article's Creative Commons licence and your intended use is not permitted by statutory regulation or exceeds the permitted use, you will need to obtain permission directly from the copyright holder. To view a copy of this licence, visit <http://creativecommons.org/licenses/by-nc-nd/4.0/>.

© The Author(s) 2025